Background prostate tissue is quantitatively abnormal on MRI in patients with clinically significant prostate cancer

Christopher C Conlin[1], Roshan Karunamuni[2], Troy S Hussain[2], Allison Y Zhong[3], Karoline Kallis[2], Deondre D Do[2,4], Asona J Lui[2], Garnier Mani[3], Courtney Ollison[5], Mariluz Rojo Domingo[4], Ahmed Shabaik[6], Christopher J Kane[7], Aditya Bagrodia[7], Rana R McKay[7,8], Joshua M Kuperman[1], Rebecca Rakow-Penner[1], Michael E Hahn[1], Anders M Dale[1,9,10], Tyler M Seibert[1,2,4]

[1]Department of Radiology, University of California San Diego School of Medicine, La Jolla, CA, USA
[2]Department of Radiation Medicine and Applied Sciences, University of California San Diego School of Medicine, La Jolla, CA, USA
[3]University of California San Diego School of Medicine, La Jolla, CA, USA
[4]Department of Bioengineering, University of California San Diego Jacobs School of Engineering, La Jolla, CA, USA
[5]Department of Biology, San Diego State University
[6]Department of Pathology, University of California San Diego School of Medicine, La Jolla, CA, USA
[7]Department of Urology, University of California San Diego School of Medicine, La Jolla, CA, USA
[8]Department of Medicine, University of California San Diego School of Medicine, La Jolla, CA, USA
[9]Department of Neurosciences, University of California San Diego School of Medicine, La Jolla, CA, USA
[10]Halıcıoğlu Data Science Institute, University of California San Diego, La Jolla, CA, USA

Running Title:
Background prostate is MRI-abnormal in cancer patients

Keywords:
Prostate cancer; T_2-weighted MRI; Background prostate tissue; Tissue characterization; Cancer detection

Financial Support:
This work was supported, in part, by the Prostate Cancer Foundation, the American Society for Radiation Oncology, and the National Institutes of Health (#K08EB026503, #UL1TR000100)

Corresponding Author:
Tyler M Seibert
Address: Altman Clinical and Translational Research Institute
9500 Gilman Drive, #0861
La Jolla, CA 92093
Telephone: (858) 246-5988
Email: tseibert@health.ucsd.edu

Conflict of Interest Disclosure:
AMD is a Founder of and holds equity in CorTechs Labs, Inc, and serves on its Scientific Advisory Board. He is a member of the Scientific Advisory Board of Human Longevity, Inc. and receives funding through research agreements with General Electric Healthcare. RRP is a consultant for Human Longevity, Inc. She also receives funding through research grants from GE Healthcare and Imagine Scientific to the University of California San Diego; she has an equity interest in CorTechs Labs, Inc. and serves on its Scientific Advisory Board. She also has equity interest in CureMetrix. TMS reports honoraria from Multimodal Imaging Services Corporation, Varian Medical Systems, and WebMD; he has an equity interest in CorTechs Labs, Inc. and serves on its Scientific Advisory Board. These companies might potentially benefit from the research results. The terms of the above arrangements have been reviewed and approved by the University of California San Diego in accordance with its conflict-of-interest policies.

Word count:
3350

Figures:
6

Tables:
2

Translational Relevance:

Diagnosis of prostate cancer has been considerably improved by the introduction of MRI. Research on this topic has focused on detecting and characterizing MRI-visible lesions, identified by comparing the lesions to the background prostate tissue. In this study, we demonstrate that the background, non-lesion prostate tissue is also abnormal on MRI in patients with cancer. This finding suggests that the MRI signal of background prostate tissue affords complementary diagnostic information to lesion-specific analysis that could improve clinical decision-making around biopsy. It also shows that MRI can inform the investigation of biological changes beyond identified index lesion(s). Whether the observed abnormalities in background prostate tissue reflect tumor-induced effects, a field effect predisposing to high-grade cancer, or some combination of both, they motivate a new line of inquiry for rad-path correlation in prostate cancer.

Abstract

Background: T_2-weighted MRI is standard for detecting clinically significant prostate cancer (csPCa) by identifying visible lesions that stand out from the background prostate.

Purpose: To determine whether patients with csPCa have abnormal T_2-weighted signal in non-lesion, background prostate tissue (BP).

Methods: This retrospective study included two patient cohorts who underwent 3T MRI examination for suspected csPCa. Median (urine-normalized) T_2-weighted signal was computed for BP and compared between patients with and without csPCa. csPCa discrimination performance of T_2-weighted BP signal was evaluated using area under receiver operating characteristic curves (AUC). T_2 and S_0 (a proxy for proton density) were computed and compared between patients with and without csPCa. T_2 was also recomputed using larger buffers around csPCa lesions. csPCa discrimination performance was compared between two predictors: Restriction Spectrum Imaging (RSI) C_1 and RSI C_1 normalized by global prostate median T_2-weighted signal.

Results: Cohort 1: 46 patients (age: 64±10 years). Cohort 2: 151 patients (65±8 years). Urine-normalized T_2-weighted signal was systematically lower in BP of subjects with csPCa ($p \leq 0.034$) and indicated the presence of cancer (cohort 1: AUC=0.80; cohort 2: AUC=0.68). BP T_2 was significantly lower in csPCa patients ($p \leq 0.011$), while S_0 was not ($p \geq 0.30$). BP T_2 measurements were stable to within 5% with buffers from 0 to 30 mm around visible lesions. csPCa discrimination improved with incorporation of BP T_2-weighted signal (cohort 1: AUC=0.72 for RSI C_1 alone, versus 0.81 with BP T_2-weighted signal; cohort 2: AUC=0.63 versus 0.76).

Conclusion: Lower T_2-weighted signal in BP suggests the presence of csPCa.

Introduction

While many studies have established the value of T_2 for detection of clinically significant prostate cancer (csPCa) (1–6), these have focused on characterizing the T_2 within radiographically visible lesions. Current practice, per standardized reporting guidelines (PI-RADS), is to compare local T_2-weighted signal to the background signal within the prostate to identify hypointense lesions that may represent csPCa. However, there are several common processes (MRI-invisible cancer, pre-cancerous lesions, inflammation, some components of benign prostatic hyperplasia, etc.) that can lead to darker T_2-weighted signal throughout the gland (7–9), thus potentially undermining the contrast of csPCa compared to the background. The present study seeks to determine whether patients with csPCa have abnormal T_2-weighted signal in prostate tissue *outside* of the index lesions identified on MRI—i.e., in the background prostate (BP).

It has long been known that csPCa arises within a field effect of histopathological abnormalities (10,11). More recently, genomic studies have demonstrated that even the benign BP in patients with csPCa has a wide range of genetic alterations (12). It is unclear to what extent BP is changed because of germline features, somatic mutations, inflammatory changes, and/or reactive processes secondary to the presence of csPCa in the gland. Identifying patients with abnormal MRI features outside visible lesions might provide insight into underlying biology. BP abnormalities could also complement lesion-level features in estimating the probability of a patient having csPCa and therefore potentially useful in deciding which patients need to undergo prostate biopsy.

Here, we test two independent patient cohorts for a systematic decrease in the T_2-weighted signal of BP in patients with csPCa. We hypothesize that T_2-weighted signal from BP can indicate the presence of csPCa. We then examine whether T_2 or proton density effects are driving the observed reduction in T_2-weighted signal, and whether these effects stem from normal age-related changes to the prostate or simply from cancer adjacent to radiological

lesions (8). Finally, we test whether T_2-weighted signal characteristics of BP provide information complementary to focal restricted diffusion-weighted MRI (DWI) to improve patient-level detection of csPCa.

Materials and Methods

Study population

This retrospective study was approved by the local institutional review board (IRB). A waiver of consent was obtained from the IRB to access patient MRI data and other clinical records. Two cohorts of patients with suspected csPCa were included in this study, independent in time and in MRI acquisition protocol. The first cohort was comprised of 81 consecutive men who underwent MRI examination on a single scanner between August and December of 2016. The second cohort included consecutive 440 men who underwent MRI examination on the same scanner between January of 2017 and February of 2020, after implementation of a change in acquisition protocol. Patients were included in analyses if they had no prior treatment for prostate cancer; in the larger cohort 2, patients were additionally excluded if they did not have a biopsy within 6 months of the MRI. Both cohorts have been studied previously for characterization of signal in lesions (13–15). BP signal has not been reported previously.

MRI acquisition

All MR imaging was performed on 3T clinical scanners (Discovery MR750; GE Healthcare, Waukesha, WI), using a 32-channel phased-array body coil surrounding the pelvis. Acquisition details are summarized in Table 1. For each patient of cohort 1, two axial DWI volumes were separately acquired using different echo times (TEs) but with other parameters held constant. For cohort 2, a single axial DWI volume was acquired for each patient. For anatomical reference, a higher resolution T_2-weighted volume was acquired for all patients, with scan coverage identical to that of the multi-shell DWI volume.

MRI data post-processing

Post-processing and analysis of all MRI data was performed using MATLAB (The MathWorks, Inc; Natick, MA). Diffusion data were first corrected for distortions due to B_0 inhomogeneity, gradient nonlinearity, and eddy currents (16–18). The multiple DWI samples acquired at each *b*-value were averaged together. To correct for patient motion between the two separately-acquired DWI volumes of cohort 1, multiscale image registration by intensity correlation was applied (19). To account for arbitrary signal-intensity scaling between acquisitions, all DWI volumes were normalized by the median signal intensity of urine in the bladder at b=0 s/mm^2 (20).

Quantitative T_2 mapping was performed for all patients of cohort 1 by fitting the signal values from the two b=0 s/mm^2 volumes acquired at different TEs with the T_2-weighted signal decay formula: $S(TE) = S_0 e^{-TE/T_2}$, where $S(TE)$ is the signal measured at a particular TE, S_0 is the signal potential at magnetic equilibrium (which is proportional to proton density (21)), and T_2 is the transverse relaxation time. Voxel-wise estimates of both T_2 and S_0 were recorded for each patient.

For all patients, regions of interest (ROIs) were defined for the whole prostate (WP), peripheral zone (PZ), and transition zone (TZ). Anatomic segmentation/contouring was performed by a radiation oncologist (3 years of experience) and two board-certified radiologists (3 and 6 years of experience, respectively) using MIM software (MIM Software, Inc; Cleveland, OH). Lesions were identified by board-certified radiologists, per clinical routine, using PI-RADS criteria. Lesion ROIs were defined for this study by consensus by two board-certified radiologists using multiparametric MRI (mpMRI) and PI-RADS v2.1. The presence or absence of csPCa (grade group ≥2) was per clinical diagnostic routine using biopsy or prostatectomy specimens.

Examination of T_2-weighted signal in BP

The median signal value on the urine-normalized b=0 s/mm^2 (i.e., T_2-weighted) volumes was computed for all ROIs (WP, PZ, and TZ) in BP. For patients without identifiable lesions (whether or not cancer was found on systematic biopsy), this amounted to calculating the median signal within the whole ROI. For patients with visible lesions, the lesion ROI was excluded from the calculation, along with an added 5-mm margin around the lesion ROI to account for the possibility of cancer outside the defined lesion ROI. Formally, the median was computed from all voxels in the set $A \cap B^C$, where A is the set of voxels in the gland ROI (WP, PZ, or TZ), B is the set of voxels within the lesion ROI dilated by 5 mm, and B^C denotes the complement of B. Median BP signal values were compared between patients with csPCa and those without csPCa using two-sample t-tests to assess statistical significance (α=0.05). Median signal values were also analogously compared between benign and cancerous lesions.

To examine the diagnostic utility of T_2-weighted signal in BP, receiver operating characteristic (ROC) curves were generated at the patient level, using median BP signal values as predictor variables to determine the presence or absence of csPCa on clinical biopsy (generally 12 systematic cores, plus targeted cores for lesions identified on MRI). ROC curves were generated for the median BP signal of each zonal ROI (WP, PZ, and TZ), as well as for the median signal of the whole gland with lesions included. The area under each ROC curve (AUC) was computed to evaluate csPCa discrimination performance.

Potential causes of BP signal differences between patients with and without csPCa

T_2-weighted signal intensity is governed by hardware factors (e.g., receiver gain) and two tissue-specific parameters: proton density (directly related to the signal potential at magnetic equilibrium, S_0) and transverse relaxation time (T_2) (21). Imaging hardware was consistent for all patients in this study, so any observed differences in T_2-weighted BP signal between subjects was assumed to arise from differences in either the proton density or T_2 of the BP.

Median T_2 (in milliseconds) was computed from the voxel-wise T_2 maps of cohort 1 within all BP ROIs to quantify the impact of T_2 on BP signal. Similarly, median S_0 was computed from the voxel-wise S_0 maps of cohort 1 within all BP ROIs to quantify the impact of proton density on BP signal. T_2 and S_0 measurements from BP were compared between patients with and without csPCa, using two-sample *t*-tests (α=0.05). T_2 and S_0 values were similarly compared between benign and cancerous lesions.

To evaluate the extent to which age-related effects might be driving any observed differences in BP characteristics between patients with and without csPCa, the Pearson correlation was computed between patient age and any BP parameters (median T_2, S_0) that were significantly different between patients with and without csPCa.

To ensure that any differences in the BP signal of patients with csPCa were not simply the result of adjacent tumor tissue that was missed during lesion contouring and erroneously included as part of the background prostate, median T_2 in the BP was computed multiple times with increasingly large buffers of excluded voxels around the csPCa lesion ROI. Specifically, the median T_2 was computed from all voxels in the set $A \cap (B + m)^C$, where A is the set of voxels in the gland ROI (WP, PZ, or TZ), B is the radiographically defined lesion ROI, and m is the buffer of excluded voxels around B. The width of the buffer m around B was increased from 0 to 30 mm in increments of one voxel-width, approximately 2.5 mm. For comparison, median T_2 was also computed for the whole gland with lesions included.

Comparison of T_2-weighted signal and diffusion in the prostate

To examine if the T_2-weighted signal characteristics of the prostate provide additional diagnostic information beyond that provided by patient-level DWI alone, T_2-weighted signal in the whole prostate was compared against a previously validated biomarker of prostate cancer based on focal diffusion restriction: Restriction Spectrum Imaging (RSI) C_1 (RSI C_1). RSI C_1 signal was computed from the DWI data of each patient by fitting with a previously described 4-

compartment RSI model (13,14). Prior studies have employed the maximum C_1 value within the prostate as a diffusion-based indicator of prostate cancer (14,15), so the maximum C_1 value within the prostate was recorded for each patient in the present study. The Pearson correlation was then computed between the median T_2-weighted signal and maximum C_1 value in the prostate. Finally, two ROC curves were generated for each patient cohort, one using only the maximum RSI C_1 as the predictor variable, and one using the maximum RSI C_1 normalized by the median T_2-weighted signal, to indicate the presence or absence of csPCa (grade group ≥2) on clinical biopsy (generally 12 systematic cores, plus targeted cores for lesions identified on MRI).

Data Availability

The data generated in this study are available upon request from the corresponding author.

Results

Study population

A flowchart illustrating patient selection for this study is shown in Figure 1. From cohort 1, 46 patients (age: 64±10 years; PSA: 10.8±17.2 ng/mL) were included. From cohort 2, 151 patients were included (age: 65±8 years; PSA: 11.8±13.9 ng/mL). Radiologic and pathologic characteristics are summarized in Table 2 for both patient cohorts.

T_2-weighted signal in BP

Figure 2 summarizes the T_2-weighted signal characteristics of prostate tissue from both cohorts. Median urine-normalized T_2-weighted signal was systematically lower in subjects with csPCa compared to those without, even in BP. In cohort 1, the observed decrease in median T_2-weighted signal was statistically significant for each of the examined anatomical zones, with p=2.5e-4 for WP, p=6.8e-4 for PZ, and p=1.3e-4 for TZ. Median T_2-weighted signal within

csPCa lesions was also significantly lower (p=0.003) compared to benign lesions. In cohort 2, the decrease in median T_2-weighted signal was significant for all zones (p=8.0e-5 for WP, p=7.6e-4 for PZ, and p=2.0e-4 for TZ), as well as for csPCa lesions compared to benign or clinically insignificant (grade group 1) prostate cancer lesions (p=0.034).

The csPCa discrimination performance of median T_2-weighted BP signal is quantified by the ROC curves in Figure 3. In cohort 1, csPCa discrimination performance was similar for BP measurements within the WP and TZ, each having an AUC value of 0.80. The AUC value for BP PZ was slightly lower: 0.77. AUC values for cohort 2 were generally lower than for cohort 1, but still indicated good classification performance of BP signal: 0.68 for WP, 0.66 for PZ, and 0.69 for TZ. In both cohorts, WP classification performance of BP only was nearly identical to the performance with lesions included. The AUCs for BP WP and WP (including lesions) were both 0.80 in cohort 1 and 0.68 in cohort 2.

Potential causes of BP signal differences between patients with and without csPCa

Figure 4 summarizes the T_2 time and S_0 characteristics of prostate tissue from cohort 1 (the only cohort for which multi-TE acquisitions were available to examine these parameters). Median T_2 was significantly lower in BP of patients with csPCa compared to those without, with p=0.002 for WP, p=2.7e-4 for PZ, and p=0.011 for TZ. Median T_2 was also significantly lower in csPCa lesions compared to benign lesions (p=0.009). Median S_0, conversely, was not significantly different in patients with csPCa compared to those without, either in BP (p=0.30 for WP, p=0.39 for PZ, p=0.33 for TZ) or lesions (p=0.30).

The T_2 of BP was not significantly correlated with patient age (Supplemental Figure 1), whether measured in the WP (Pearson r=-0.02, p=0.91), PZ (Pearson r=-0.15, p=0.32), or TZ (Pearson r=0.16, p=0.30).

BP T_2 measurements from patients with csPCa were relatively insensitive to changes in the size of the margin around the csPCa lesion ROI that was excluded from the BP T_2

calculation (Figure 5). BP T_2 values were stable within 5% for margin values 0 to 30 mm. BP T_2 measurements changed by a maximum of 4.8% in the WP, 4.8% in the PZ, and -4.1% in the TZ. With lesions included in the measurement, WP and TZ T_2 values were 0.7% lower than the values measured from BP only. PZ T_2 was 4.1% lower with lesions included.

Comparison of T_2-weighted signal and RSI C_1 in the whole prostate

Supplemental Figure 2 plots whole-prostate measures of maximum RSI C_1 (previously shown to be predictive of patient-level csPCa) against median urine-normalized T_2-weighted signal. No significant correlation was observed between the two metrics in either cohort (cohort 1: Pearson r=-0.01, p=0.96; cohort 2: Pearson r=0.08, p=0.36). Consideration of T_2-weighted signal along with RSI C_1 yielded improved cancer discrimination performance compared to RSI C_1 alone (Figure 6). In cohort 1, the AUC increased from 0.72 for maximum RSI C_1 alone to 0.81 for maximum RSI C_1 normalized by median T_2-weighted signal. In cohort 2, the AUC increased from 0.63 to 0.76.

Discussion

To our knowledge, this is the first study to specifically examine *background* prostate tissue for abnormal T_2 relaxation associated with the presence of csPCa in the prostate. We found that T_2-weighted signal intensity in the BP of patients with csPCa was systematically lower than in patients without csPCa. This systematic decrease in T_2-weighted BP signal was observed across two different patient cohorts that were independently acquired using different imaging protocols, suggesting that it is not an artifact of experimental design. Furthermore, T_2-weighted signal in the BP meaningfully discriminated patients with or without csPCa, perhaps surprising considering current clinical practice focuses exclusively on suspicious lesions. The csPCa discrimination performance achieved using T_2-weighted signal in the BP alone was comparable

to the performance reported for methods that examine signal properties within radiographically identified lesions (22–24).

We considered a few explanations for cancer-associated T_2-weighted signals observed in BP in both cohorts. First, we noted that T_2-weighted signals could be driven by differences in proton density, but multi-TE data from cohort 1 revealed no association of S_0 in BP with csPCa. Meanwhile, there was a significant decrease in the apparent T_2 time of the BP in patients with csPCa compared to those without. Second, normal age-related changes in prostate T_2 have been described (25), but we found no correlation here between BP T_2 and patient age. Third, we know that csPCa can be present adjacent to visible lesions (8). Though the median T_2 should not be influenced too heavily by inclusion of a relatively small tumor in the BP ROI, we computed the BP T_2 value multiple times with increasingly large buffers of excluded voxels around the lesion ROI. If tumor tissue adjacent to the prescribed lesion contour were driving the observed decrease in median BP T_2, we would expect that increasing the buffer around the contour would significantly increase the recorded BP T_2 values and eliminate the systematic difference between patients with csPCa and those without. However, we found the median BP T_2 to be largely insensitive to the lesion buffer size, making lesion-adjacent cancer an unlikely explanation for BP signal differences.

Patients with csPCa may have abnormal BP for several reasons: (1) MRI-invisible cancer not adjacent to the MRI-visible lesion; (2) a field effect of prostate changes possibly related to predisposition to csPCa; and/or (3) reactive changes to the presence of csPCa in part of the gland. The existence of MRI-invisible cancer is well known (26–28), though csPCa is more likely to be near MRI-visible lesions and would be encompassed by our buffer analyses (8). csPCa is also known to arise in the context of a field effect of prostate-wide conditions that predispose to oncogenesis (11). T_2 changes in BP might reflect pre-cancerous changes, including inflammation, chemical irritation, pathogen exposure, and/or modifications in local gene expression (29). A recent study described striking genomic alterations of benign prostate

tissue in patients with csPCa (12). Future studies should leverage advanced quantitative imaging techniques like luminal water imaging (2) and MR spectroscopy (30) to better assess the T_2 properties of BP in patients with and without csPCa. Regardless of etiology, the abnormal BP in patients harboring csPCa suggests the presence of interesting biological processes beyond what is reflected in MRI-visible lesions.

T_2-weighted signal in BP contributes meaningful information and may have diagnostic or prognostic clinical value. We have previously shown that a quantitative DWI biomarker called RSI C_1 is useful for voxel-level and patient-level detection of csPCa (14,15). Median T_2 in the prostate was not correlated with maximum RSI C_1, and patient-level csPCa detection improved after normalizing maximum RSI C_1 by median T_2. These findings suggest T_2 signal of the entire prostate, not just of the radiographically visible lesions, may provide insight into the physiological changes linked to csPCa and may improve risk stratification of patients with suspected prostate cancer. As a practical consideration for incorporating this information into clinical practice, we demonstrated that median T_2 measurements from the entire prostate (visible lesions included) were largely indistinguishable from median values of the BP alone, with nearly identical csPCa detection performance. Whole-prostate contouring is relatively simple and can now be performed automatically with freely-available AI tools (31), obviating the need for expert delineation of lesions by specialized radiologists in order to integrate BP signal information into diagnostic decision making.

Classification performance differed between Cohort 1 and Cohort 2. This may simply reflect chance variation, but there are some noteworthy differences between the cohorts that reflect dynamic patterns in clinical practice over time. The chronologically more recent Cohort 2 included proportionally more patients with a prior biopsy. Cohort 2 also had more patients with targeted-only biopsy. Perhaps most importantly, when the data from Cohort 2 was being acquired, urologists at our institution had become increasingly reliant on MRI results in deciding which patients to biopsy, such that Cohort 2 had zero participants with PI-RADS 1 lesions,

compared to over 20% of Cohort 1. Inclusion of more PI-RADS 1 patients would be expected to improve the performance of MRI, and the AUC for Cohort 1 was indeed higher than for Cohort 2.

A limitation of this study is that proton density weighted data were not acquired for the patients included in this study, so we could not directly examine the proton density of BP. However, since imaging hardware was fixed across all patients, tissue proton density should be the principal determinant of S_0. Limitations of retrospective studies also apply. This was a single-center, single-scanner study, though two different acquisition protocols were used. Future studies will also leverage whole-mount histopathology and explore molecular and genomic alterations associated with T_2 abnormalities in benign and benign-appearing tissue.

We conclude that the background tissue of the prostate exhibits systematically abnormal T_2-weighted MRI in patients who harbor csPCa. This global prostate effect appears complementary to the focal diffusion restriction characteristic of suspicious visible lesions. In sum, MRI signal outside visible lesions may afford untapped diagnostic value for detection of csPCa. These intriguing initial findings should be validated in broader datasets.

References

1. Mai J, Abubrig M, Lehmann T, et al. T2 Mapping in Prostate Cancer. Investigative Radiology. 2019;54(3):146–152. doi: 10.1097/RLI.0000000000000520.

2. Sabouri S, Chang SD, Savdie R, et al. Luminal Water Imaging: A New MR Imaging T2 Mapping Technique for Prostate Cancer Diagnosis. Radiology. Radiological Society of North America; 2017;284(2):451–459. doi: 10.1148/radiol.2017161687.

3. Metzger GJ, Kalavagunta C, Spilseth B, et al. Detection of Prostate Cancer: Quantitative Multiparametric MR Imaging Models Developed Using Registered Correlative Histopathology. Radiology. Radiological Society of North America; 2016;279(3):805–816. doi: 10.1148/radiol.2015151089.

4. Hoang Dinh A, Souchon R, Melodelima C, et al. Characterization of prostate cancer using T2 mapping at 3T: A multi-scanner study. Diagnostic and Interventional Imaging. 2015;96(4):365–372. doi: 10.1016/j.diii.2014.11.016.

5. Roebuck JR, Haker SJ, Mitsouras D, Rybicki FJ, Tempany CM, Mulkern RV. Carr-Purcell-Meiboom-Gill imaging of prostate cancer: quantitative T2 values for cancer discrimination. Magnetic Resonance Imaging. 2009;27(4):497–502. doi: 10.1016/j.mri.2008.08.001.

6. Hoang Dinh A, Melodelima C, Souchon R, et al. Quantitative Analysis of Prostate Multiparametric MR Images for Detection of Aggressive Prostate Cancer in the Peripheral Zone: A Multiple Imager Study. Radiology. Radiological Society of North America; 2016;280(1):117–127. doi: 10.1148/radiol.2016151406.

7. Rourke E, Sunnapwar A, Mais D, et al. Inflammation appears as high Prostate Imaging–Reporting and Data System scores on prostate magnetic resonance imaging (MRI) leading to false positive MRI fusion biopsy. Investig Clin Urol. 2019;60(5):388–395. doi: 10.4111/icu.2019.60.5.388.

8. Brisbane WG, Priester AM, Ballon J, et al. Targeted Prostate Biopsy: Umbra, Penumbra, and Value of Perilesional Sampling. European Urology. 2022;82(3):303–310. doi: 10.1016/j.eururo.2022.01.008.

9. Guneyli S, Ward E, Thomas S, et al. Magnetic resonance imaging of benign prostatic hyperplasia. Diagn Interv Radiol. 2016;22(3):215–219. doi: 10.5152/dir.2015.15361.

10. Deutsch E, Maggiorella L, Eschwege P, Bourhis J, Soria JC, Abdulkarim B. Environmental, genetic, and molecular features of prostate cancer. The Lancet Oncology. 2004;5(5):303–313. doi: 10.1016/S1470-2045(04)01468-8.

11. Bostwick DG, Shan A, Qian J, et al. Independent origin of multiple foci of prostatic intraepithelial neoplasia. Cancer. 1998;83(9):1995–2002. doi: 10.1002/(SICI)1097-0142(19981101)83:9<1995::AID-CNCR16>3.0.CO;2-2.

12. Erickson A, He M, Berglund E, et al. Spatially resolved clonal copy number alterations in benign and malignant tissue. Nature. Nature Publishing Group; 2022;608(7922):360–367. doi: 10.1038/s41586-022-05023-2.

13. Conlin CC, Feng CH, Rodriguez-Soto AE, et al. Improved Characterization of Diffusion in Normal and Cancerous Prostate Tissue Through Optimization of Multicompartmental Signal Models. Journal of Magnetic Resonance Imaging. 2021;53(2):628–639. doi: https://doi.org/10.1002/jmri.27393.

14. Feng CH, Conlin CC, Batra K, et al. Voxel-level Classification of Prostate Cancer on Magnetic Resonance Imaging: Improving Accuracy Using Four-Compartment Restriction Spectrum Imaging. Journal of Magnetic Resonance Imaging. 2021;54(3):975–984. doi: 10.1002/jmri.27623.

15. Zhong AY, Digma LA, Hussain T, et al. Patient-level detection of grade group ≥2 prostate cancer using quantitative diffusion MRI. medRxiv. 2021;2021.05.24.21256461. doi: 10.1101/2021.05.24.21256461.

16. Holland D, Kuperman JM, Dale AM. Efficient correction of inhomogeneous static magnetic field-induced distortion in Echo Planar Imaging. NeuroImage. 2010;50(1):175–183. doi: 10.1016/j.neuroimage.2009.11.044.

17. White NS, McDonald CR, Farid N, et al. Diffusion-Weighted Imaging in Cancer: Physical Foundations and Applications of Restriction Spectrum Imaging. Cancer Res. 2014;74(17):4638–4652. doi: 10.1158/0008-5472.CAN-13-3534.

18. Zhuang J, Hrabe J, Kangarlu A, et al. Correction of Eddy-Current Distortions in Diffusion Tensor Images Using the Known Directions and Strengths of Diffusion Gradients. J Magn Reson Imaging. 2006;24(5):1188–1193. doi: 10.1002/jmri.20727.

19. Paquin D, Levy D, Schreibmann E, Xing L. Multiscale Image Registration. Mathematical Biosciences & Engineering. 2006;3(2):389. doi: 10.3934/mbe.2006.3.389.

20. Sunoqrot MRS, Nketiah GA, Selnæs KM, Bathen TF, Elschot M. Automated reference tissue normalization of T2-weighted MR images of the prostate using object recognition. Magn Reson Mater Phy. 2021;34(2):309–321. doi: 10.1007/s10334-020-00871-3.

21. Bloch F. Nuclear Induction. Phys Rev. American Physical Society; 1946;70(7–8):460–474. doi: 10.1103/PhysRev.70.460.

22. Bajgiran AM, Mirak SA, Sung K, Sisk AE, Reiter RE, Raman SS. Apparent Diffusion Coefficient (ADC) Ratio Versus Conventional ADC for Detecting Clinically Significant Prostate Cancer With 3-T MRI. American Journal of Roentgenology. American Roentgen Ray Society; 2019;213(3):W134–W142. doi: 10.2214/AJR.19.21365.

23. Singh S, Rogers H, Kanber B, et al. Avoiding Unnecessary Biopsy after Multiparametric Prostate MRI with VERDICT Analysis: The INNOVATE Study. Radiology. Radiological Society of North America; 2022;212536. doi: 10.1148/radiol.212536.

24. Lee GH, Chatterjee A, Karademir I, et al. Comparing Radiologist Performance in Diagnosing Clinically Significant Prostate Cancer with Multiparametric versus Hybrid Multidimensional MRI. Radiology. Radiological Society of North America; 2022;211895. doi: 10.1148/radiol.211895.

25. Bura V, Caglic I, Snoj Z, et al. MRI features of the normal prostatic peripheral zone: the relationship between age and signal heterogeneity on T2WI, DWI, and DCE sequences. Eur Radiol. 2021;31(7):4908–4917. doi: 10.1007/s00330-020-07545-7.

26. Ahdoot M, Wilbur AR, Reese SE, et al. MRI-Targeted, Systematic, and Combined Biopsy for Prostate Cancer Diagnosis. New England Journal of Medicine. Massachusetts Medical Society; 2020;382(10):917–928. doi: 10.1056/NEJMoa1910038.

27. Rouvière O, Puech P, Renard-Penna R, et al. Use of prostate systematic and targeted biopsy on the basis of multiparametric MRI in biopsy-naive patients (MRI-FIRST): a prospective, multicentre, paired diagnostic study. The Lancet Oncology. 2019;20(1):100–109. doi: 10.1016/S1470-2045(18)30569-2.

28. Ahmed HU, El-Shater Bosaily A, Brown LC, et al. Diagnostic accuracy of multi-parametric MRI and TRUS biopsy in prostate cancer (PROMIS): a paired validating confirmatory study. The Lancet. 2017;389(10071):815–822. doi: 10.1016/S0140-6736(16)32401-1.

29. Schillaci O, Scimeca M, Trivigno D, et al. Prostate cancer and inflammation: A new molecular imaging challenge in the era of personalized medicine. Nuclear Medicine and Biology. 2019;68–69:66–79. doi: 10.1016/j.nucmedbio.2019.01.003.

30. Taneja SS. Imaging in the Diagnosis and Management of Prostate Cancer. Rev Urol. 2004;6(3):101–113.

31. Belue MJ, Turkbey B. Tasks for artificial intelligence in prostate MRI. Eur Radiol Exp. 2022;6:33. doi: 10.1186/s41747-022-00287-9.

Table 1: MRI acquisition details for the two patient cohorts included in this study. DWI volumes were acquired using a diffusion-weighted spin-echo pulse sequence (default tensor) with an echo-planar imaging (EPI) readout. T_2-weighted (T2W) volumes were acquired using a fast spin-echo (FSE) pulse sequence. In-phase and out-of-phase T_1-weighted images were acquired using "Liver Acquisition with Volume Acquisition (LAVA)-Flex," a dual-echo, fast spoiled gradient-echo sequence. Water-only and fat-only images were generated automatically from the in-phase/out-of-phase images by scanner software using the 2-point Dixon method. Dynamic contrast-enhanced (DCE) MRI was performed using a time-resolved imaging of contrast kinetics (TRICKS) protocol with a temporal resolution of one frame every 7 seconds. Baseline-subtracted volumes were automatically generated from TRICKS data by the scanner software.

		FOV (mm)	Matrix [resampled dimensions]	Slices	Slice thickness (mm)	TR (ms)	TE (ms)	b-values (s/mm^2) [number of samples]
Cohort 1	DWI 1	220×220	96×96 [128×128]	34	3	5000	80	0 [7*], 200 [6], 1000 [6], 2000 [6], 3000 [6]
	DWI 2	220×220	96×96 [128×128]	34	3	5000	100	0 [7*], 200 [6], 1000 [6], 2000 [6], 3000 [6]
	T2W	220×220	320×320 [512×512]	34	3	6225	100	N/A
	T1 LAVA-Flex	320×256	320×224 [512×512]	140	4	4	2 (in-phase) 1 (out-of-phase)	N/A
	DCE	220×220	256×168 [512×512]	32	3	4	2	N/A
Cohort 2	DWI	240×120	96×48 [128×64]	16	6	4500	68	0 [2*], 500 [6], 1000 [6], 2000 [12]
	T2W	240×240	320×320 [512×512]	32	3	6080	102	N/A
	T1 LAVA-Flex	340×272	320×224 [512×512]	140	4	4	2 (in-phase) 1 (out-of-phase)	N/A
	DCE	240×240	256×168 [512×512]	64	3	4	2	N/A

*An extra b=0 s/mm^2 volume was acquired with reverse phase encoding to enable correction of B_0-inhomogeneity distortions

Table 2: Summary of radiologic and pathologic characteristics of the two patient cohorts included in this study.

		Cohort 1	Cohort 2
Previous biopsy	Biopsy naïve	38	103
	Past biopsy	8	48
Available pathology	Systematic biopsy only	28	7
	Targeted biopsy only	0	17
	Systematic and targeted biopsy	15	85
	No biopsy*	3	0
	Prostatectomy	12	42
PI-RADS score†	1	10	0
	2	2	5
	3	10	27
	4	10	55
	5	14	64
Gleason Grade Group	None	23	29
	1	3	39
	2	8	35
	3	7	20
	4	1	16
	5	4	12

*In the smaller Cohort 1, three patients did not have biopsy but had normal MRI and low clinical suspicion of csPCa.
†PI-RADS v2 was used for cohort 1, PI-RADS v2.1 for cohort 2

Figures and Figure Legends

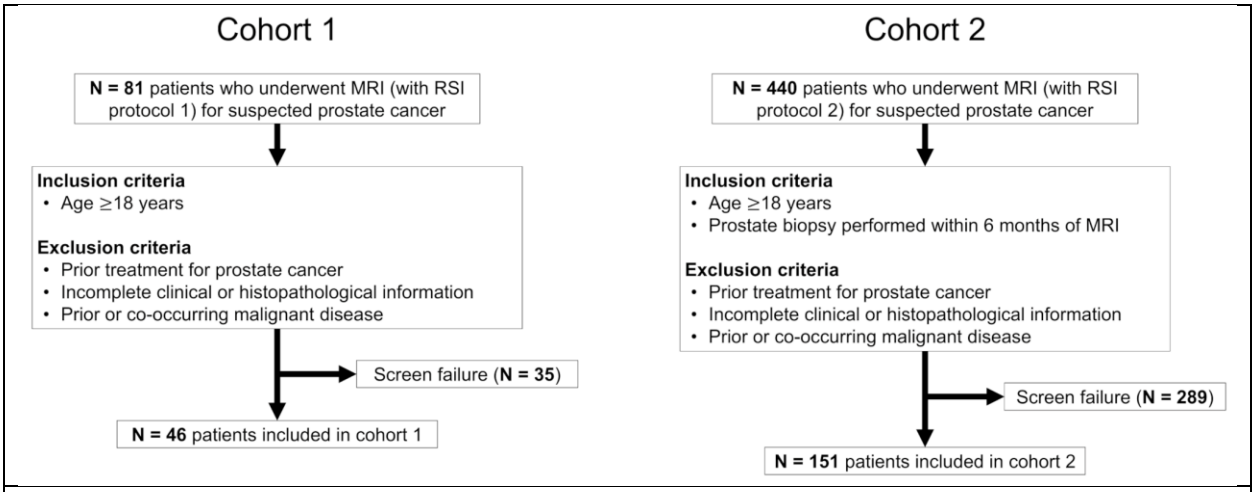

Figure 1: Flowchart illustrating patient selection for both cohorts considered for this study.

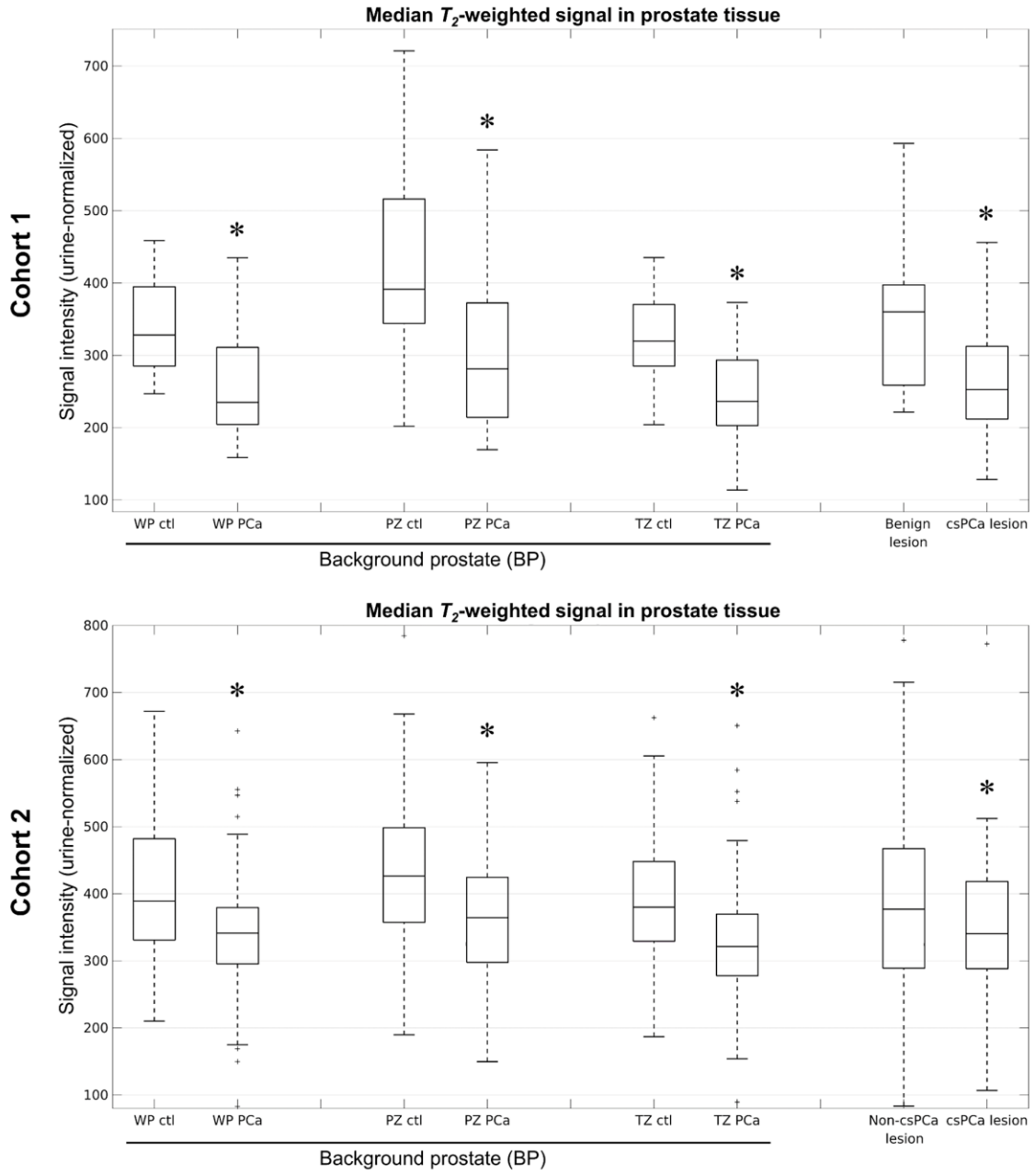

Figure 2: T_2-weighted signal in prostate tissue of subjects with and without clinically significant prostate cancer (csPCa). Median (urine-normalized) T_2-weighted signal was systematically lower in subjects with csPCa, even in background prostate (BP). Asterisks indicate a significant (p<0.05) decrease in the median T_2-weighted signal of patients with csPCa compared to those without. WP: whole-prostate, PZ: peripheral zone, TZ: transition zone, ctl: control subject without csPCa, PCa: subject with csPCa. In cohort 2, the "Non-csPCa lesion" group is comprised of subjects with either a benign or clinically insignificant (grade group 1) prostate cancer lesion.

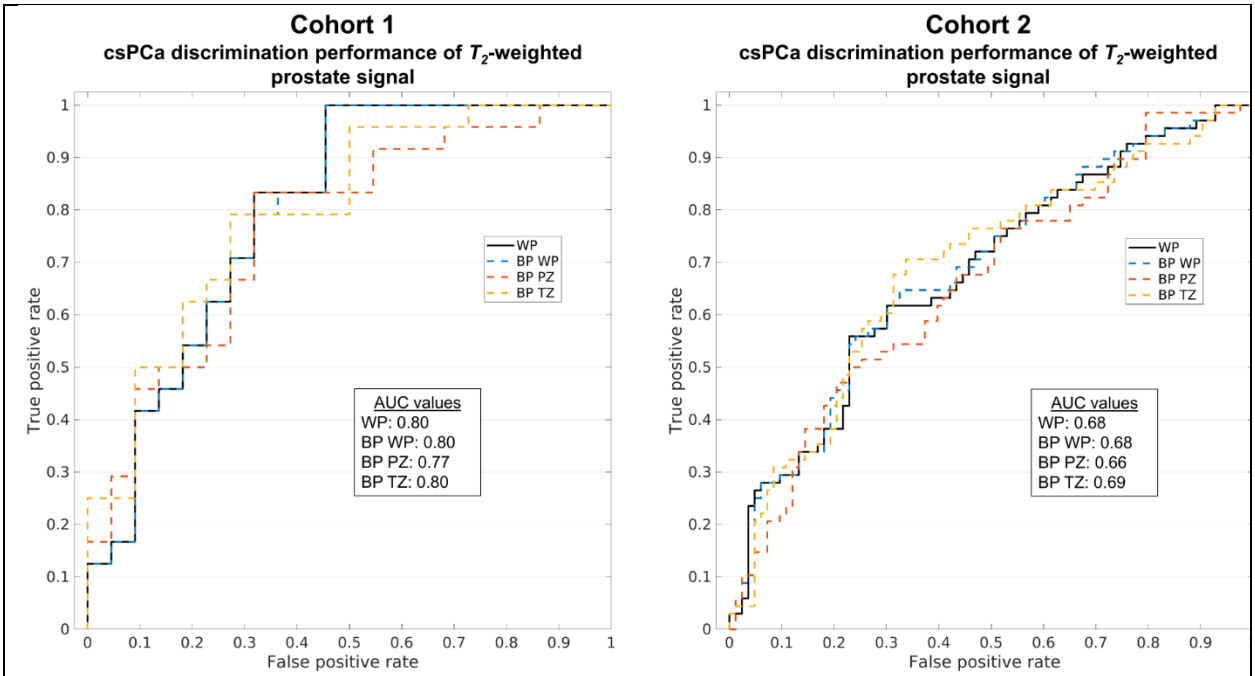

Figure 3: Receiver operating characteristic (ROC) curves illustrating the clinically significant prostate cancer (csPCa) discrimination performance of median (urine-normalized) T_2-weighted signal in background prostate (BP). The ROC curve for the whole prostate, including lesions, is shown for comparison (WP). AUC: area under the ROC curve, WP: whole-prostate, PZ: peripheral zone, TZ: transition zone.

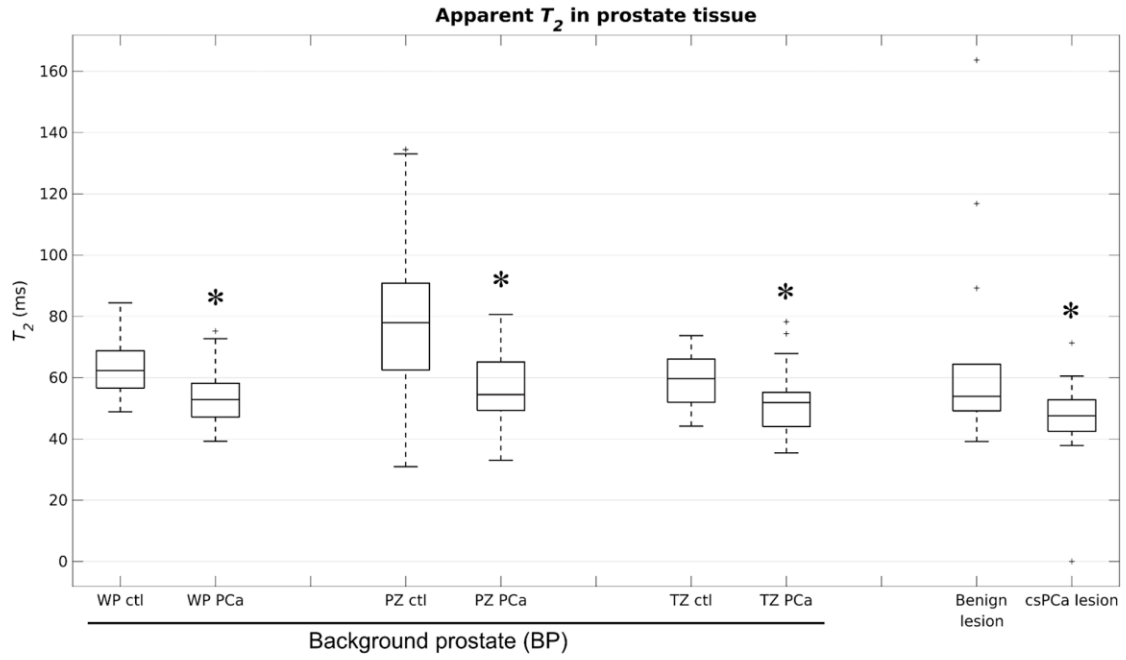

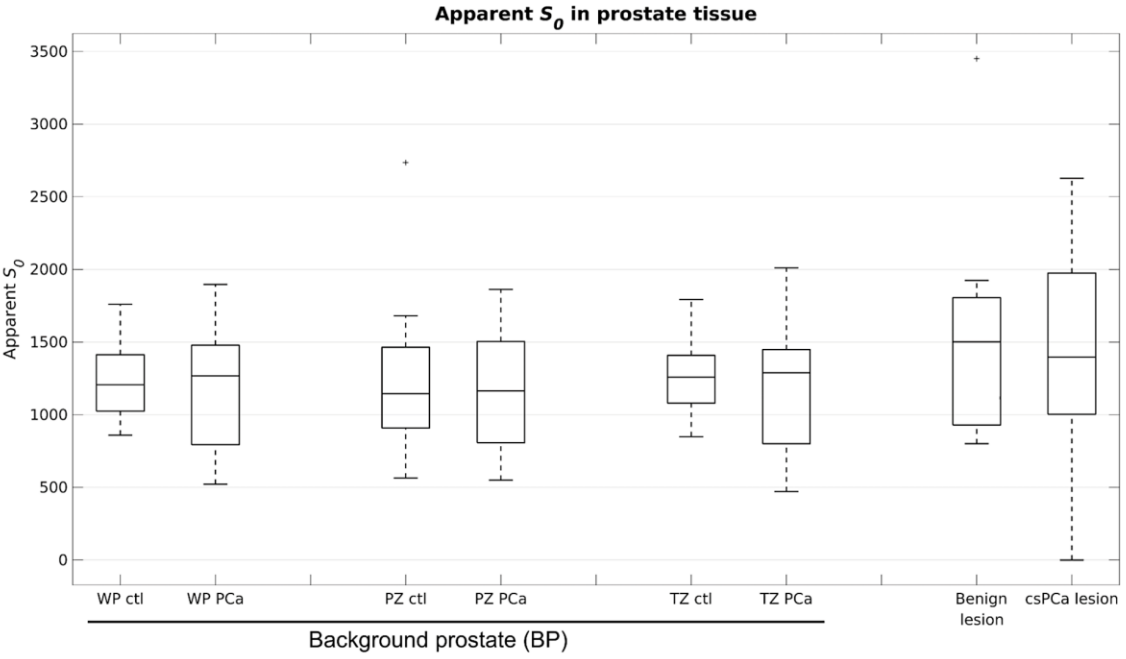

Figure 4: T_2 time and S_0 in prostate tissue of subjects from cohort 1 with and without clinically significant prostate cancer (csPCa). Asterisks indicate a significant (p<0.05) decrease in the measured value from patients with csPCa compared to those without.

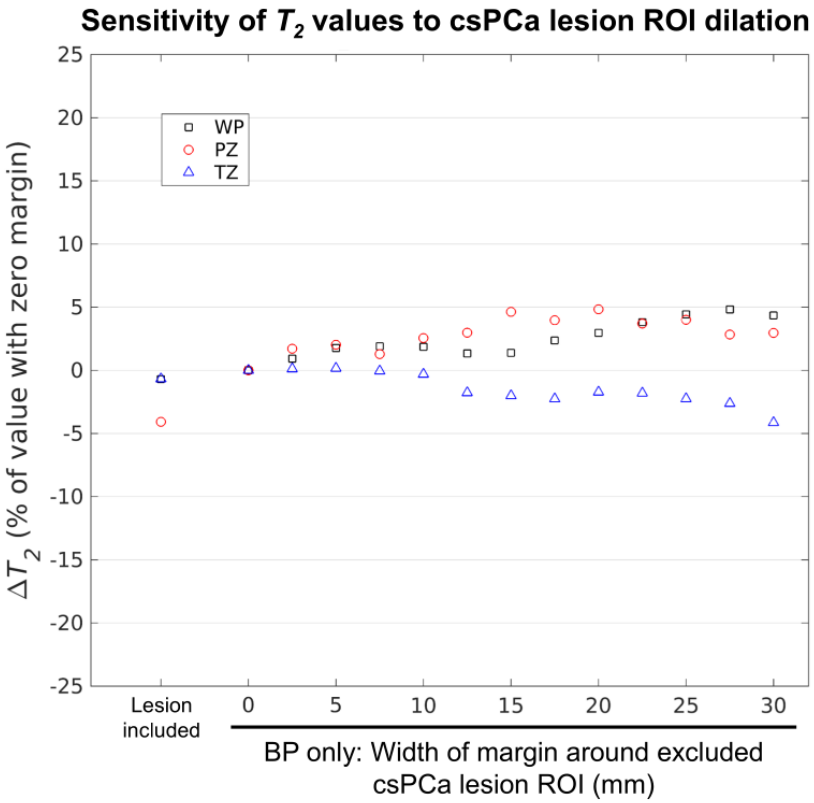

Figure 5: Sensitivity of BP T_2 measurements from cohort 1 to the width of the margin around the clinically significant prostate cancer (csPCa) lesion ROI that was excluded from the measurement. For margin widths ranging from 0 to 30 mm, BP T_2 measurements were stable to within 5%. BP T_2 changed by a maximum of 4.8% in the WP, 4.8% in the PZ, and -4.1% in the TZ. Absolute BP T_2 values for a margin width of zero were 52 ms for the WP, 54 ms for the PZ, and 52 ms for the TZ. T_2 measurements that included the lesion ROIs are shown for comparison.

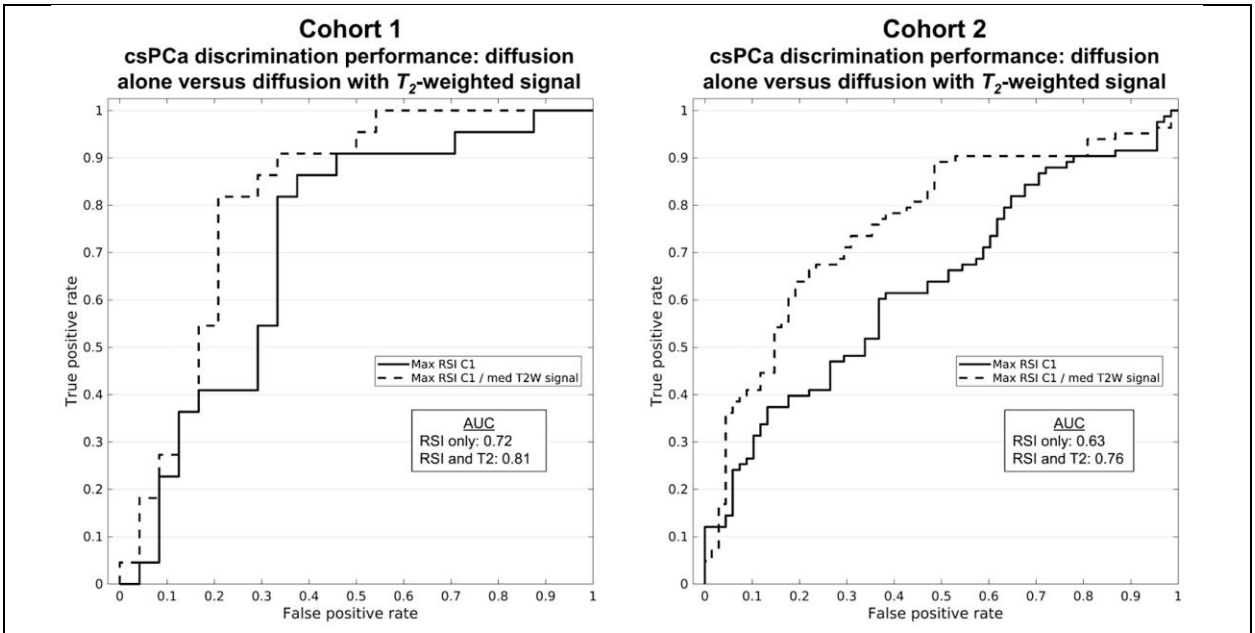

Figure 6: Receiver operating characteristic (ROC) curves illustrating the clinically significant prostate cancer (csPCa) discrimination performance of whole-prostate RSI C_1 alone versus whole-prostate RSI C_1 normalized by median T_2-weighted (T2W) signal. AUC: area under the ROC curve.

Supplemental Materials

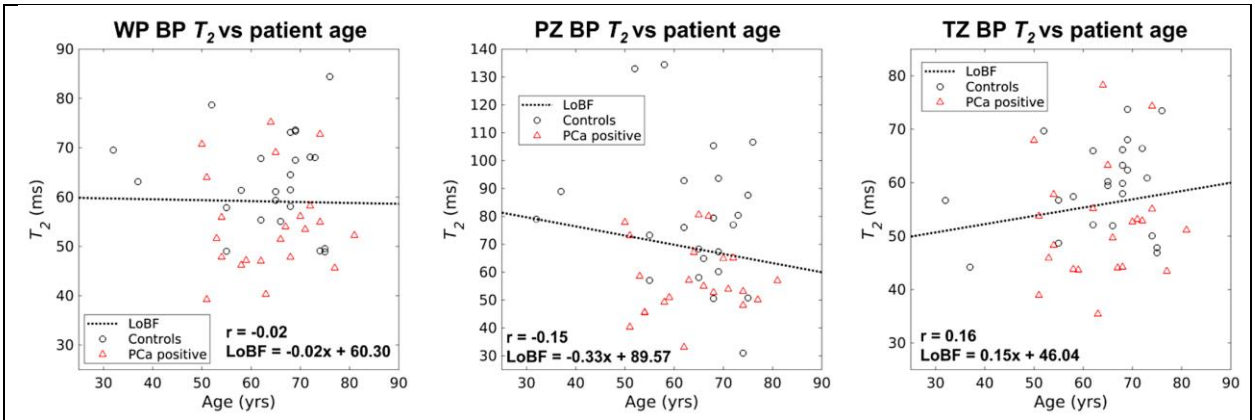

Supplemental Figure 1: Correlation of T_2 time in BP with patient age in cohort 1. T_2 was not significantly correlated with patient age in any of the prostatic zones (p>0.05 for WP, PZ, and TZ). r: Pearson correlation coefficient, LoBF: line-of-best-fit to the data.

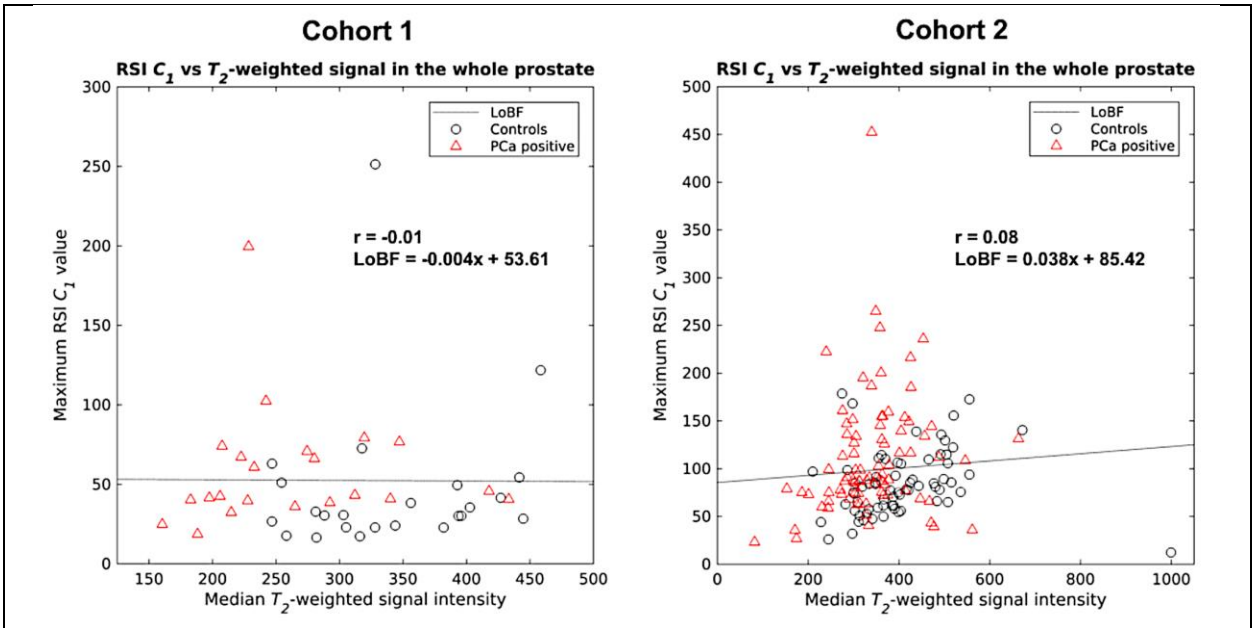

Supplemental Figure 2: Scatterplots comparing whole-prostate measurements of maximum RSI C_1 and median T_2-weighted signal intensity. No significant correlation was observed between the two metrics in either cohort (p>0.05). r: Pearson correlation coefficient, LoBF: line-of-best-fit to the data.